Metasurface-Based Holographic Display With All-Dielectric Meta-Axilens

Chuan Shen [ID], Rulin Xu [ID], Jiali Sun [ID], Zhuang Wang, and Sui Wei

Abstract—In a classical metasurface-based holographic display system, a clear holographic reconstruction image can be obtained only in the back-focal-plane of the lens. However, when the receiving plane deviates from the focal plane, the reconstructed holographic image suffers from degradations that limit the quality of the images. Hence, we propose a novel metasurface-based holographic display to realize clearly continuous imaging within the specified position range by superimposing the meta-axilens phase. It can effectively relieve the alignment requirements of the imaging system. Firstly, the parameters and properties of all-dielectric meta-atom is analyzed. Then we compare and demonstrate two sets of metasurface-based optical elements (meta-axicon, meta-lens, and meta-axilens), made by silicon meta-atoms working at 610 nm. Furthermore, we show that the metasurface hologram with the axilens phase can form a series of the relatively clear holographic images away from the focal plane. Our proposal suggests a method to reconstruct holographic wavefront in different planes simultaneously, and one can find their application domain, such as 3D biological imaging, spectroscopy, optical information storage, and encryption.

Index Terms—Metasurface, holographic display, meta-axilens.

I. INTRODUCTION

AS AN important application of metasurface, metasurface optical elements have the properties of ultra-thin, ultra-light, miniaturization, and planarization. They are expected to replace existing traditional optical lens manufactured based on geometric optics in the fields of optical lithography [1], laser-based microscopy [2], and spectroscopy [3]. This will be a huge revolution in the miniaturization, portability, and wearability of optical components again. Furthermore, the metasurfaces perform more light field control dimensions than traditional diffractive optical elements, so optical elements with more innovative functions can be manufactured by metasurface. On the other hand, the metasurface also promotes the leaping development of holographic display technology [4], [5], [6],

[7], [8]. It breaks through the diffraction limit of the traditional spatial light modulator (SLM), such as liquid crystal on silicon (LCoS) [9], bringing a larger holographic field of view (FOV) and more flexible control dimensions [10], [11]. Especially in recent years, metasurface-based holographic display enjoys dramatic improvements in both the concept and the technology, improvements that vastly extended its applicability and practicality, respecting to complex-amplitude metasurface [12], full-color holographic display with multi-freedom manipulate metasurface [13] and dynamic display of vectorial holography based on metasurface [14], etc. Theoretically, if hologram is expected to image in the region very close to the source, it can be observed in the back focal plane through a lens. However, the sub-wavelength structure and micron-scale scale of the metasurfaces brings precision control problems. Therefore, an optical element in micro-nano scale is urgently needed to expand the depth of metasurface-based holographic display.

Of the metasurface-based technologies that have been explored over recent years, the meta-lens has shown several amazing properties (e.g., imaging resolution, magnification, and focusing efficiency), that are very useful for optical systems [15]. However, the meta-lens is also extremely sensitive to the imaging distance and position due to the lack of long depth of focus. On the other hand, axicon performs a long depth of focusing operation and can produce non-diffracted light, such as Bessel beams, which are widely used in optical imaging, optical tweezers, and optical processing [16], [17]. Therefore, the axicon has sufficient long depth of focal but also has low lateral resolution. Whereas, axilens can effectively reduce the accuracy of the distance between the imaging lens and the sensor because it shares the properties of both lens and axicon [18], [19]. Recently, researchers have carried out research on the planarization and programming of axilens, and axilens has been applied to holographic projection based on LCoS [20], spectroscopy [21], [22], optical fabrication [23], and other fields. Inspired by the meta-lens and the meta-axicon, we could use metasurface to construct the meta-axilens. We ultimately wish to form a metasurface-based holographic image in good focus, not only in the back-focal-plane of the lens, but also in the neighbourhood of this plane.

In this work, we proposed a metasurface-based holographic display method with a meta-axilens. The main idea is that the phase-only hologram generated by the iterative Fourier transform algorithm (IFTA) is superposed with the axilens to obtain a new phase distribution, which is then employed to encode a new all-dielectric metasurface, so that a single metasurface can performs the high lateral resolution of the lens and the long focal depth of the axicon simultaneously. Firstly, the parameters and properties of meta-atom is analyzed. Then, we compared and demonstrated the modulation capability of two sets of silicon
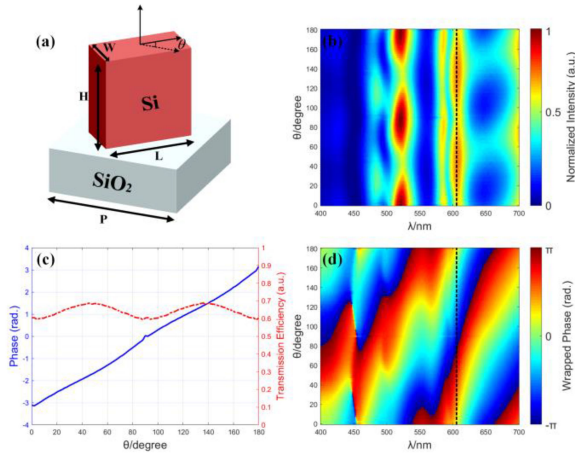
Fig. 1. (a) Schematic diagram of the silicon meta-atom (P = 300 nm, L = 200 nm, H = 200 nm, W = 100 nm). (b) & (d) Normalized intensity and wrapped phase distribution of the output wavefront when λ and θ change. (c) Transmission efficiency and phase of the output wavefront with change at $\lambda = 610$ nm.

dielectric metasurface optical element (meta-axicon, meta-lens, and meta-axilens) with similar parameters. Finally, simulations based on FDTD methods show the imaging results of metasurface holograms optimized by the axilens phase in a number of selected receiving planes.

II. META-AXILENS

The metasurface structures are based on a geometry related to the meta-atom, the designed meta-atom is shown in Fig. 1(a). Based on the principle of Pancharatnam−Berry (PB) phase [24], the PB phase is introduced by changing the rotation angle θ of the nanobrick to modulate incident light and it can realize the phase control of a wide spectrum as shown in Fig. 1(d). Each silicon nanobrick of optical antenna is located on the quartz substrate and has same length L = 200 nm, width W = 100 nm, and height H = 200 nm. The period size of the meta-atoms is 300 nm. According to the Jones matrix representation of the PB phase, the incident light selects the left circularly polarized light (LCP), and the modulation effect will be reflected in the right circularly polarized light (RCP). In order to analyze the light field response, we use finite-difference time-domain technique (FDTD) method based on commercial solver (FDTD Solutions, Lumerical) to sweep the wavelength λ of incident light and rotation angle θ of optical antenna. Fig. 1(b) and (d) present normalized intensity and wrapped phase of the output light when λ and θ change. As shown in Fig. 1(c), meta-atom has $0 \sim 2\pi$ complete phase modulation capabilities, and the normalized intensity reaches $\sim 70\%$ at the wavelength of 610 nm (indicated by the vertical dashed line in Fig. 1(b) and (d)).

Taking account of the illumination of circularly polarized light, the Jones matrix of the PB phase principle is of the form,

$$\begin{bmatrix} E_{xout} \\ E_{yout} \end{bmatrix} = \frac{\boldsymbol{J}_\theta}{\sqrt{2}} \begin{bmatrix} 1 \\ i\sigma \end{bmatrix}$$

$$= \frac{1}{\sqrt{2}} \begin{bmatrix} t_u\cos^2\theta + t_v\sin^2\theta & (t_u - t_v)\sin\theta\cos\theta \\ (t_u - t_v)\sin\theta\cos\theta & t_u\sin^2\theta + t_v\cos^2\theta \end{bmatrix} \begin{bmatrix} 1 \\ i\sigma \end{bmatrix}$$

$$= \frac{1}{2\sqrt{2}} \left\{ (t_u + t_v) \begin{bmatrix} 1 \\ i\sigma \end{bmatrix} + (t_u - t_v)\exp(2i\sigma\theta) \begin{bmatrix} 1 \\ -i\sigma \end{bmatrix} \right\} \quad (1)$$

where, the output light is $\begin{bmatrix} E_{xout} \\ E_{yout} \end{bmatrix}$, $\boldsymbol{J}_\theta$ is jones matrix, $\sigma = \pm 1$ denotes the LCP and RCP, respectively. t_u and t_v are the transmittances on different symmetry axes of nanobrick, respectively.

Now consider the phase profile of an axilens, which is defined by [18],

$$\varphi_{Axilens}(r) = \frac{\pi}{\lambda} \frac{r^2}{f_0 + \frac{Z_g}{R^2}r^2} \quad (2)$$

where, λ is the wavelength of the incident light, R is the radius of the axilens, $r = \sqrt{x^2 + y^2}$ is the radial coordinate f_0 and Z_g are the focal length and the focal depth of axilens respectively. In addition, considering the comparison with the meta-lens and meta-axicon that follows, the phase functions of the lens and the axicon are also given,

$$\varphi_{Lens}(x, y) = \frac{2\pi}{\lambda}(\sqrt{(x^2 + y^2) + f^2} - f) \quad (3)$$

where, f is the focal length of lens.

$$\varphi_{Axicon} = \frac{2\pi}{\lambda}\sqrt{x^2 + y^2}\frac{R}{\sqrt{Z_g^2 + R^2}} \quad (4)$$

where, Z_g and R are the focal depth of axicon and the radius of axicon respectively.

Utilizing the previous meta-atom, we design a sets of metasurface optical elements including meta-lens, meta-axicon, meta-axilens. The focal length of meta-lens is $f = 60$ μm, the focal depth of meta-axicon is $Z_g = 20$ μm, the focal length and the focal depth of axilens are $f_0 = 60$ μm and $Z_g = 20$ μm, respectively. In addition, all optical elements have the same diameter with the incident light of 45.3 μm. It should be noted that the above parameters are aimed at providing a reference basis for the design of metasurface-based axilenses and holograms that follows.

Fig. 2 illustrates the simulated optical field results along the propagation direction, respectively. The meta-lens has the highest intensity distribution at the focal position, where the light field is effectively converged, hence, it has a higher lateral resolution. The output light field of the meta-axicon offers a characteristic of long focal length, showing a good Bessel beam generation effect. Compared with the meta-lens, the meta-axilens has a longer focal depth near the focal length, it achieves continuous convergence within the focal depth range and shows similar non-diffraction characteristics. Through measurement, the Full Width at Half Maximum (FWHM) of the meta-lens and the meta-axilens in the simulations are 7.94 μm and 17.01 μm, respectively.

Fig. 3 illustrates a series of simulations of the normalized intensity distributions behind the lens and axilens at different planes normal to the propagation z axis. As shown in Fig. 3(right), by comparison of these intensity distributions, it is evident that the intensity distribution of the central part for the meta-axilens remains close to the same spot size in the depth of focal range, whereas it cannot offer the same results for their counterpart meta-lens.

III. METASURFACE HOLOGRAM WITH META-AXILENS

The previous meta-atom can also be used as holographic materials to encode computer-generated holograms (CGH). As a kind of sub-wavelength optical element, the sufficient condition for far-field diffraction would indicate that the distance be several
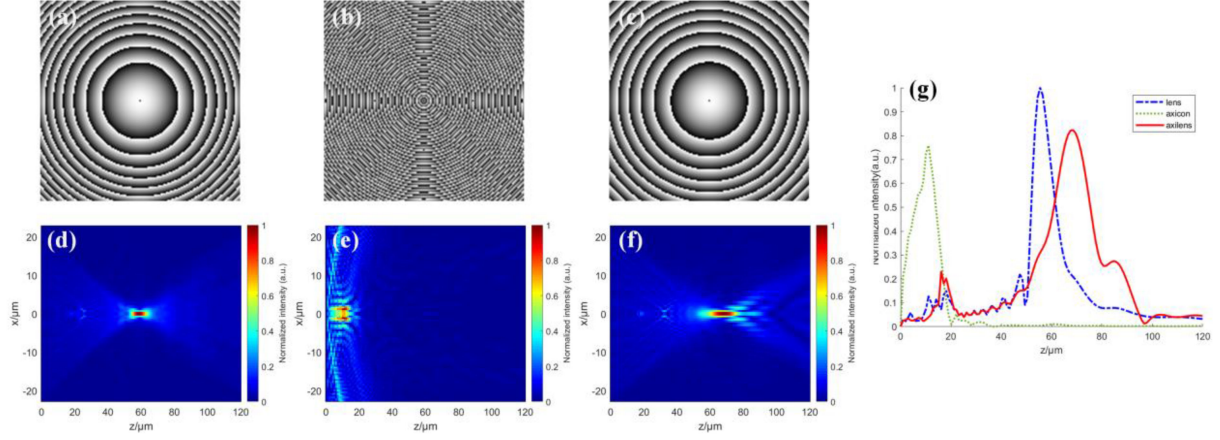
Fig. 2. FDTD simulation results of metasurface optical elements (lens $f = 60\ \mu$m, axicon $Z_g = 20\ \mu$m and axilens $f_0 = 60\ \mu$m, $Z_g = 20\ \mu$m). (a), (b), (c) illustrate the phase profile (indicated by gray scale) of the lens, axicon, and axilens, respectively. (d), (e), (f) illustrate the cross-section intensity distribution along the propagation direction of the lens, axicon, and axilens, respectively. (g) illustrates the comparison of intensity distribution corresponding to optical element (lens, axicon and axilens) with propagation distance.
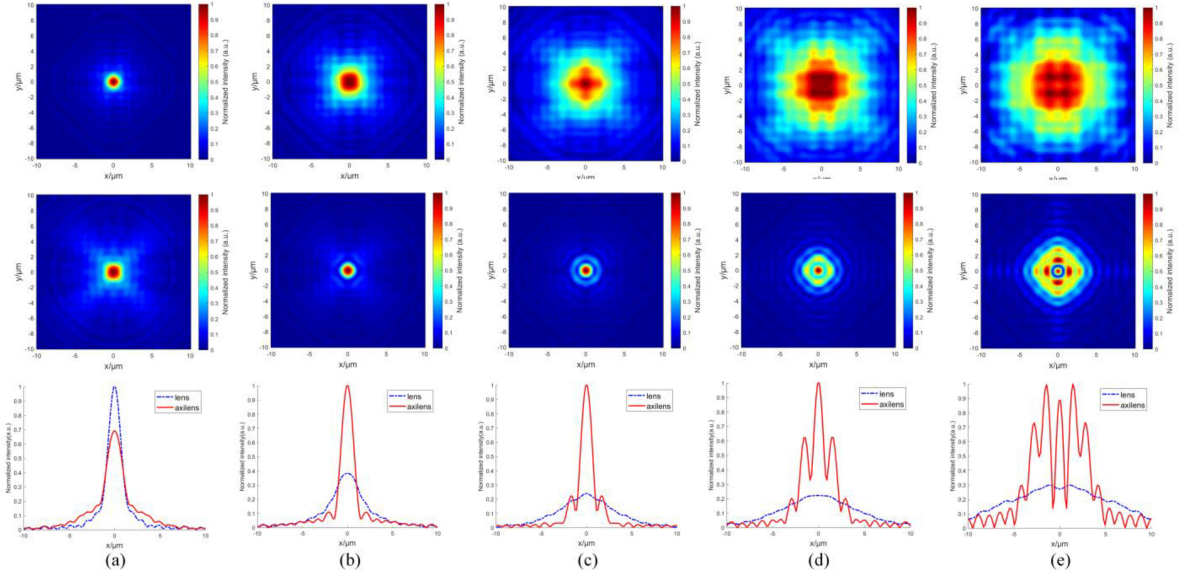

Fig. 3. Simulated intensity distributions of the lens (top), axilens (middle) and the comparison of the intensity cross sections (bottom) at several distances from the meta-lens and meta-axilens. (a) $Z = 60\ \mu$m. (b) $Z = 65\ \mu$m. (c) $Z = 70\ \mu$m. (d) $Z = 75\ \mu$m. (e) $Z = 80\ \mu$m.

millimeters, so the far-field reconstruction of meta-hologram could be realized without a lens. On the other hand, by superimposing the phase of meta-lens, the receiving plane or sensor needs to be accurately placed on the focal plane. This is not an engineerable high-precision batch operation. Therefore, we propose a method to extend the imaging range of the hologram by using a meta-axilens to achieve continuous imaging within the focal depth range. The phase of the hologram optimized by superimposing the axilens phase is used to encode the all-dielectric metasurface,

$$\varphi_{metasurface} = \mathrm{mod}(\varphi'_{hologram} + \varphi_{Axilens}, 2\pi) \quad (5)$$

where, the phase $\varphi_{metasurface}$ of hologram optimized by axilens is reduced by modulo 2π.

In simulations, we choose the "AHU" (abbreviation of Anhui University) image with 151×151 pixels as the original target image, and IFTA algorithm is used to calculate the corresponding

phase-only hologram of target image [25]. As shown in Fig. 4, the phase profile of the axilens mentioned above is superimposed to hologram of "AHU". Consider that the full-mode simulation of FDTD consumes a high cost of time and computer memory. Before performing a series of simulations based on FDTD method, it will be helpful to first state the simulation parameters preliminarily based on scalar diffraction theory for the case of combination both the hologram and the axilens. The Huygens-Fresnel principle, as predicted by the first Rayleigh-Sommerfeld solution can be adopted to calculate the light propagation. Since all optical elements have the same diameter 45.3 μm, which is large compared with a wavelength of 610 nm. Meanwhile, the focal plane is not too close to each optical element. Finally, the Fresnel approximation could be used for simplicity. Two sets of metasurface optical elements including lens, axicon, axilens are simulated. In the former case, the parameters of the lens, axicon and axilens are unchanged. In the latter case, the focal length of
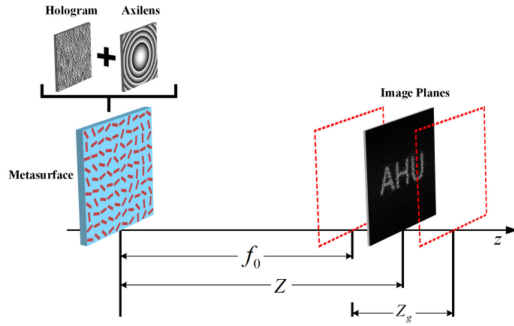
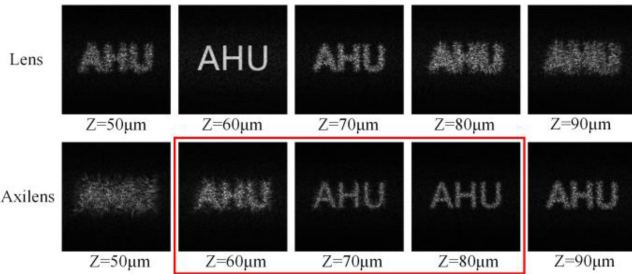Fig. 4. Schematic diagram of the metasurface-based holographic display system at different observation plane.

Fig. 5. Simulated reconstruction images of superimposed the phase of meta-lens (focal length $f = 60\ \mu$m) and the phase of meta-axilens (focal length $f_0 = 60\ \mu$m, focal depth $Z_g = 20\ \mu$m).
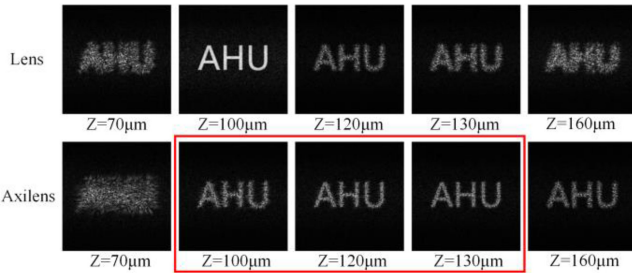

Fig. 6. Simulated reconstruction images of superimposed the phase of meta-lens (focal length $f = 100\ \mu$m) and the phase of meta-axilens (focal length $f_0 = 100\ \mu$m, focal depth $Z_g = 40\ \mu$m).

meta-lens is $f = 100\ \mu$m, the focal depth of meta-axicon is $Z_g = 40\ \mu$m, the focal length and the focal depth of axilens are $f_0 = 100\ \mu$m and $Z_g = 40\ \mu$m, respectively.

For our simulations, the intensity distribution in a number of injected receiving planes near focus are computed. As shown in Fig. 5 and Fig. 6, the hologram with lens phase only has a high quality imaging result at the back focal plane. The hologram with an axilens phase compared with a lens phase can still maintain a relatively clear image in the range of the focal depth (marked by the red wire frame). Corresponding to the two sets of simulations above, a number of holographic images are also calculated with step change of 2 μm at propagation distance from 50 μm to 120 μm for the former case, and the same number of samples is taken for the latter case. As shown in Fig. 7, the peak signal-to-noise ratio (PSNR) also quantifies the
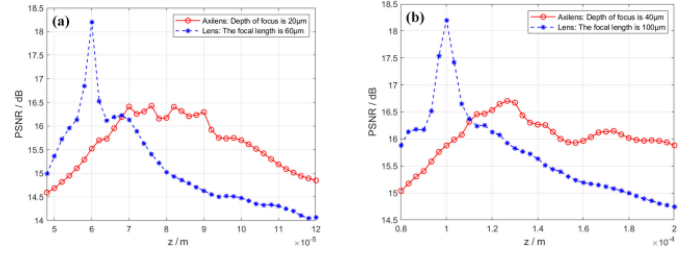

Fig. 7. PSNR value as a function of the axial distance around the focal region for the axilens and a lens. (a) focal length $f_0 = 60\ \mu$m, focal depth $Z_g = 20\ \mu$m. (b) focal length $f_0 = 100\ \mu$m, focal depth $Z_g = 40\ \mu$m.

above conclusions. Unfortunately, due to the characteristics of the axilens, it concentrates only a small fraction of the energy into the focused beam, which results in an extremely low PSNR value than the lens at the constant focal plane. It should be emphasized that the above simulation can be regarded as an auxiliary simple correspond to the central simulations to be discussed in the following sections. Because the period size of the meta-atoms is 300nm, that is smaller than the size of a wavelength 610nm, so the fundamentally vectorial nature of the electromagnetic fields should probably be needed. It will be not quite accurate if we still use a scalar theory to predict the optical phenomena of our structure.

Now by considering the FDTD method with the above parameters, we perform full-mode verification on metasurface holograms superimposed by the axilens phases. Fig. 8 illustrate the intensity distributions of the output light field in a number of selected receiving planes. The result is straightforward, although the constraint of computer resource leads to a lower data sampling resolution. We see that for the case of a meta-lens, as shown in Fig. 8(a), the simulated holographic image "AHU" that can be clear in the focal plane of the lens but suffers from degradations significantly with distance away from the above plane. Attention is paid to the case of a meta-axilens, with the two sets of the previous parameters, as shown in Fig. 8(b) and Fig. 8(c), we could still identify the "AHU" characters from reconstructed images in the range of the focal depth.

It should be noted that the trade-offs in metasurface-based holographic display simulations between holographic image quality and computing power sometimes force designers to sacrifice holographic image quality, so it must be admitted that our work is limited by the number of meta-atoms and has not achieved perfect display results, but the existing results can still prove the effectiveness of this method. With the increase in the number of modulation units, higher quality holographic images can be obtained. On the other hand, in practice it is necessary to quantize both the amplitude and the phase of a complex amplitude hologram, a process that leads to noise in the reconstructed image. As shown in Fig. 1(c), the transmission and phase error of the silicon meta-atoms also lead to scarification of the holographic image quality. Note that in our simulations, only the phase of the hologram is used to encode the all-dielectric metasurface, and the amplitude information is entirely eliminated. Furthermore, by introducing the phase of axilens instead of the lens, we could maintain a relatively clear image in the range of the focal depth, but the image quality is sacrificed to gain the long focal distances.
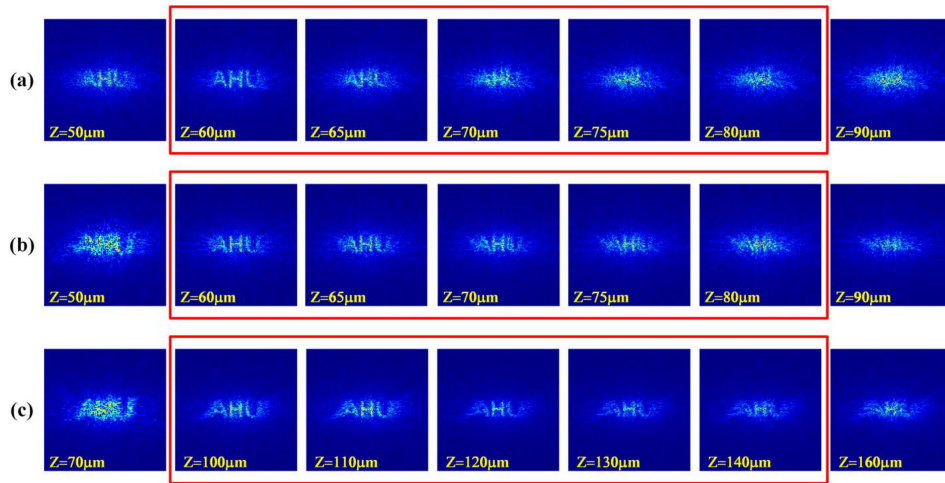
Fig. 8. The FDTD simulated reconstructed images of the holographic metasurface at different distances with (a) lens ($f = 60\ \mu$m). (b) axilens (focal length $f_0 = 60\ \mu$m, focal depth $Z_g = 20\ \mu$m). (c) axilens (focal length $f_0 = 100\ \mu$m, focal depth $Z_g = 40\ \mu$m).

IV. CONCLUSION

In conclusion, we employ the all-dielectric metasurface to realize the design of the meta-axilens, and it works at the visible light, which has a longer depth of focal than the classic meta-lens. Meta-axilens can effectively reduce the alignment requirements of the metasurface-based holographic display system. Furthermore, compared with the classical metasurface-based holographic displays, we could obtain a series of relatively clear holographic reconstructed images in the depth of focal range. Last but not least, we believe that the proposed meta-axilens can be used as a universal metasurface optical element, and it will have great application potential in the fields of 3D biological imaging, spectroscopy, optical information storage, and encryption, etc.

REFERENCES

[1] J. Luo *et al.*, "Fabrication of anisotropically arrayed nano-slots metasurfaces using reflective plasmonic lithography," *Nanoscale*, vol. 7, no. 44, pp. 18805–18812, Oct. 2015.

[2] A. Tittl *et al.*, "Imaging-based molecular barcoding with pixelated dielectric metasurfaces," *Science*, vol. 360, no. 6393, pp. 1105–1109, Jun./Aug. 2018.

[3] S. Romano *et al.*, "Surface-enhanced raman and fluorescence spectroscopy with an all-dielectric metasurface," *J. Phys. Chem. C*, vol. 122, no. 34, pp. 19738–19745, 2018.

[4] L. Huang *et al.*, "Three-dimensional optical holography using a plasmonic metasurface," *Nat. Commun.*, vol. 4, no. 1, Nov. 2013, Art. no. 2808.

[5] L. Huang *et al.*, "Broadband hybrid holographic multiplexing with geometric metasurfaces," *Adv. Mater.*, vol. 27, no. 41, pp. 6444–6449, Sep. 2015.

[6] X. Duan, S. Kamin, and N. Liu, "Dynamic plasmonic colour display," *Nat. Commun.*, vol. 8, no. 1, Feb. 2017, Art. no. 14606.

[7] Z. Deng *et al.*, "Diatomic metasurface for vectorial holography," *Nano Lett.*, vol. 18, no. 5, pp. 2885–2892, Mar. 2018.

[8] G. Lee *et al.*, "Complete amplitude and phase control of light using broadband holographic metasurfaces," *Nanoscale*, vol. 10, no. 9, pp. 4237–4245, Dec. 2018.

[9] Y. Tong, M. Pivnenko, and D. Chu, "Improvements of phase linearity and phase flicker of phase-only LCoS devices for holographic applications," *Appl. Opt.*, vol. 58, no. 34, pp. G248–G255, Dec. 2019.

[10] X. Li *et al.*, "Multicolor 3D meta-holography by broadband plasmonic modulation," *Sci. Adv.*, vol. 2, no. 11, Nov. 2016, Art. no. 1601102.

[11] J. Li, S. Kamin, G. Zheng, F. Neubrech, S. Zhang, and N. Liu, "Addressable metasurfaces for dynamic holography and optical information encryption," *Sci. Adv.*, vol. 4, no. 6, Jun. 2018, Art. no. 6768.

[12] Q. Jiang, L. Cao, H. Zhang, and G. Jin, "Improve the quality of holographic image with complex-amplitude metasurface," *Opt. Exp.*, vol. 27, no. 23, pp. 33700–33708, Nov. 2019.

[13] Z. Deng *et al.*, "Full-color complex-amplitude vectorial holograms based on multi-freedom metasurfaces," *Adv. Funct. Mater.*, vol. 30, no. 21, Mar. 2020, Art. no. 1910610.

[14] S. Zhang *et al.*, "Dynamic display of full-stokes vectorial holography based on metasurfaces," *ACS Photon.*, vol. 8, no. 6, pp. 1746–1753, May 2021.

[15] M. Khorasaninejad, W. T. Chen, R. C. Devlin, J. Oh, A. Y. Zhu, and F. Capasso, "Metalenses at visible wavelengths: Diffraction-limited focusing and subwavelength resolution imaging," *Science*, vol. 352, no. 6290, pp. 1190–1194, Jun. 2016.

[16] F. Aieta *et al.*, "Aberration-free ultrathin flat lenses and axicons at telecom wavelengths based on plasmonic metasurfaces," *Nano Lett.*, vol. 12, no. 9, pp. 4932–4936, Jul. 2012.

[17] W. T. Chen *et al.*, "Generation of wavelength-independent subwavelength bessel beams using metasurfaces," *Light Sci. Appl.*, vol. 6, no. 5, Dec. 2017, Art. no. e16259.

[18] N. Davidson, A. Friesem, and E. Hasman, "Holographic axilens: High resolution and long focal depth," *Opt. Lett.*, vol. 16, no. 7, pp. 523–525, Apr. 1991.

[19] J. Sochacki, S. Bará, Z. Jaroszewicz, and A. Kołodziejczyk, "Phase retardation of the uniform-intensity axilens," *Opt. Lett.*, vol. 17, no. 1, pp. 7–9, Jan. 1992.

[20] C. Shen, Q. Hong, Q. Zhu, C. Zu, and S. Wei, "Holographic projection based on programmable axilens," *Opt Laser Technol*, vol. 120, no. 26, Dec. 2019, Art. no. 105682.

[21] Y. Chen, W. A. Britton, and L. Dal Negro, "Phase-modulated axilenses for infrared multiband spectroscopy," *Opt. Lett.*, vol. 45, no. 8, pp. 2371–2374, Mar. 2020.

[22] Y. Chen, W. A. Britton, and L. Dal Negro, "Design of infrared microspectrometer based on phase-modulated axilenses," *Appl. Opt.*, vol. 59, no. 18, pp. 5532–5538, May 2020.

[23] D. Pan *et al.*, "Efficient fabrication of a high-aspect-ratio AFM tip by one-step exposure of a long focal depth holographic femtosecond axilens beam," *Opt. Lett.*, vol. 45, no. 4, pp. 897–900, Jan. 2020.

[24] J. C. Gutiérrez-Vega, "Pancharatnam-berry phase of optical systems," *Opt. Lett.*, vol. 36, no. 7, pp. 1143–1145, Apr. 2011.

[25] R. W. Gerchberg, "A practical algorithm for the determination of phase from image and diffraction plane pictures," *Optik*, vol. 35, pp. 237–250, Nov. 1972.